



## Multicomponent Extensive Air Shower observations at EAS-TOP

THE EAS-TOP COLLABORATION: M. Aglietta<sup>a,b</sup>, B. Alessandro<sup>b</sup>, P. Antonioli<sup>c</sup>, F. Arneodo<sup>d,e</sup>, L. Bergamasco<sup>b,f</sup>, M. Bertina<sup>b,f</sup>, A. Campos Fauth<sup>g</sup>, C. Castagnoli<sup>a,b</sup>, A. Castellina<sup>a,b</sup>, A. Chiavassa<sup>b,f</sup>, G. Cini Castagnoli<sup>b,f</sup>, B. D’Ettore Piazzoli<sup>h</sup>, G. Di Sciascio<sup>h</sup>, W. Fulgione<sup>a,b</sup>, P. Galeotti<sup>b,f</sup>, P.L. Ghia<sup>a,b</sup>, M. Iacovacci<sup>h</sup>, A. Lima de Godoi<sup>g</sup>, G. Mannocchi<sup>a,b</sup>, C. Melagrana<sup>b,f</sup>, N. Mengotti Silva<sup>g</sup>, C. Morello<sup>a,b</sup>, G. Navarra<sup>b,f</sup>, H. Nogima<sup>g</sup>, L. Riccati<sup>b</sup>, O. Saavedra<sup>b,f</sup>, G.C. Trinchero<sup>a,b</sup>, P. Vallania<sup>a,b</sup>, S. Vernetto<sup>a,b</sup>, C. Vigorito<sup>b,f</sup>

<sup>a</sup>Istituto di Cosmo-Geofisica del CNR, Corso Fiume 4, 10133 Torino, Italy

<sup>b</sup>Istituto Nazionale di Fisica Nucleare, Via Pietro Giuria 1, 10125 Torino, Italy

<sup>c</sup>Istituto Nazionale di Fisica Nucleare, Via Irnerio 46, 40126 Bologna, Italy

<sup>d</sup>Dipartimento di Fisica dell’ Università dell’Aquila, Via Vetoio, 67010 L’Aquila, Italy

<sup>e</sup>INFN Laboratori Nazionali del Gran Sasso, S.S. 17 bis, 67010 Assergi (AQ), Italy

<sup>f</sup>Dipartimento di Fisica Generale dell’ Università, Via P. Giuria, 1, 10125 Torino, Italy

<sup>g</sup>Istituto di Fisica, Universidade Estadual, Barao Geraldo, 13081 Campinas (SP), Brazil

<sup>h</sup>Dipartimento di Scienze Fisiche dell’ Università and INFN, Mostra D’Oltremare, 80125 Napoli, Italy

The study of cosmic rays at primary energies  $E_0 > 10^{14}$  eV requires the detection of the different components of Extensive Air Showers through ground based stations. EAS-TOP is such an array (located at Campo Imperatore, 2000 m a.s.l., National Gran Sasso Laboratories), including detectors of the electromagnetic, muon ( $E_\mu \approx$  GeV at the surface, and  $E_\mu \approx$  TeV in coincidence with the detectors operating in the underground Gran Sasso Laboratories), hadron and atmospheric Cerenkov light components. The combined operation of the detectors is discussed from the point of view of the capability of measuring the cosmic ray primary spectrum and composition. The main lines for checking the significant features of the high energy hadron interaction model used for the interpretation of the data are outlined.

### 1. INTRODUCTION

At primary energies above  $E_0 \approx 10^{14}$  eV the cosmic ray primary intensity becomes too low ( $I(> E_0) \approx 0.27(E_0/10^{14} \text{ eV})^{-1.65} / \text{m}^2 \text{ hr sr}$ ) to allow statistically significant measurements of the primary spectrum and composition through the direct calorimetric experiments operating on balloons or satellites. Measurements have therefore to be performed through the detection of the secondaries (Extensive Air Showers, EAS) that the primary cosmic rays produce in their interactions in the atmosphere.

Major problems of such measurements are connected with:

- the necessity of defining the “beam” geometry;
- the nature of the observation, at fixed atmospheric, i.e. target, depth;

- the steepness of the primary spectrum;
- the lack of direct knowledge of the features of secondary production in hadron interactions (p-p and p-A: cross sections, correlations and fluctuations) in the energy range and kinematic region of interest;

- the low event rate at the highest energies.

As main consequences:

- long observation times are required, with high stability detectors (often conflicting with their environmental locations, possibly at mountain altitudes);
- measurements are strongly affected by fluctuations, so that, to create a “minimum bias” sample, different EAS components have to be recorded;
- such a requirement is strengthened by the need of having the additional informations necessary to check the main features of the hadron

interaction model used to interpret the data.

Obviously, the requirement of the contemporaneous detection of different EAS components reduces the statistical sample, especially in the case of high energy secondaries, for which the detection of the core region is required, or of Cerenkov light observations having a reduced duty cycle. Such events are however of main significance for the interpretation of the full data set.

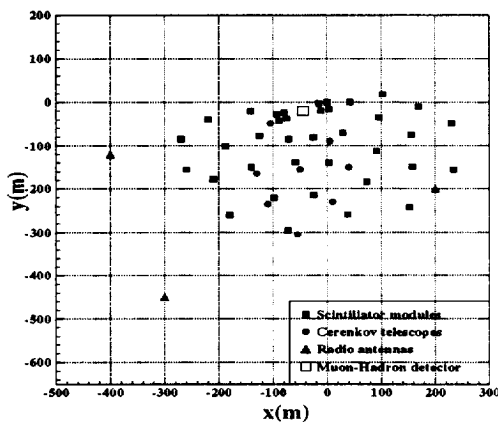


Figure 1. The EAS-TOP array.

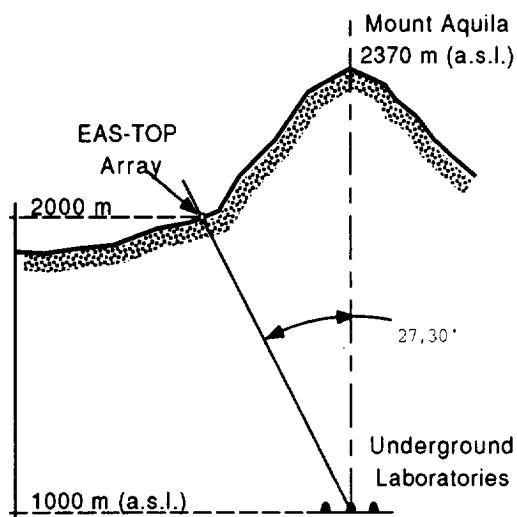


Figure 2. The EAS-TOP array location with respect to the underground Gran Sasso laboratories.

The EAS-TOP array [1] (Campo Imperatore, 2000 m a.s.l.,  $810 \text{ g cm}^{-2}$  atmospheric depth, National Gran Sasso Laboratories) has therefore been planned to detect the electromagnetic (e.m.), muon ( $E_{\mu}^{GeV}: E_{\mu} > 1 \text{ GeV}$ ), hadron, atmospheric Cerenkov light, radio emission components of Extensive Air Showers. Moreover, its location has been chosen to have the further possibility of running in coincidence with the muon detectors operating inside the deep underground Gran Sasso laboratories ( $E_{\mu}^{TeV}: E_{\mu} > 1.4 \text{ TeV}$ ).

We will discuss here the characteristics of the individual detectors and the performances of the full array in the event reconstruction, concerning the geometry and the characteristics of the cascades relevant for the studies of primary composition, and the checks of the models used for the high energy processes. While, of course, the full interpretation of the data is performed through a complete program of simulation, including the cascades in the atmosphere and the detectors responses, we will outline here the main significance of each individual measurement.

## 2. THE ARRAY AND THE METHODS

The array structure is shown in fig. 1 and fig. 2, also in connection with the underground Gran Sasso laboratories.

### 2.1. The e.m. detector

The e.m. detector [2,3] is made of 35 scintillator modules ( $10 \text{ m}^2$  each, 4 cm thick, divided into 16 individual units), organized in circles (of radii  $r = 50\text{--}80 \text{ m}$ ) interconnected with each other, for trigger and data taking organization. The events used in the following discussion are those with at least 7 detectors fired (one located at the center and six on the quoted circle), and the maximum particle density recorded by a module internal to the edges of the array. The EAS arrival direction is obtained through the times of flight among the different detectors, measured with 0.5 ns sensitivity, the precision in the response of the single scintillator to a single particle being  $\delta t = 1.3 \text{ ns}$ . The accuracy in the measurement of the arrival direction, obtained through the internal consistency of the data, is shown in fig. 3, as a function

of the shower size  $N_e$ . These resolutions are verified in celestial coordinates (thus including possible systematic effects) by the observation of the "shadow" cast by the moon on the flux of the primary cosmic rays [4]; this is shown in fig. 4, and provides a resolution of  $\sigma_\alpha = 0.83 \pm 0.10^\circ$  [5] for all events and vertical incidence, thus confirming the data reported in fig. 3.

Also shown in fig. 3 is the resolution obtained

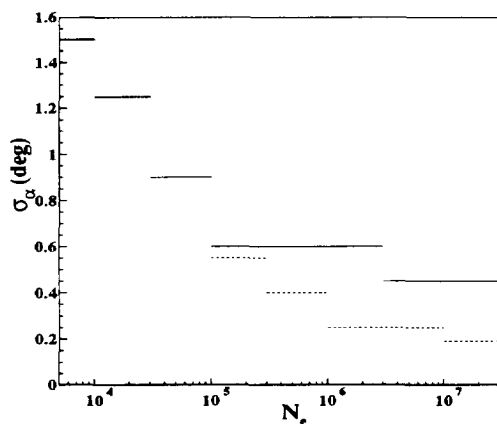


Figure 3. The angular resolution of the e.m. detector; the dotted line represents the resolution for events with core location in the central part.

for events with core internal to the second ring of modules. For large shower sizes (in order that detectors located at about 140 m from the core are fired too) the saturation in  $\sigma_\alpha$  is removed, and an accuracy  $\sigma_\alpha \approx 0.2^\circ$  is achieved at  $N_e \approx 10^6$ .

The shower size  $N_e$  and the core location are obtained from the fit to the recorded particle densities. The resolutions are obtained by means of simulations that include all experimental uncertainties [2,3]. The results are shown in figs. 5 and 6 (the resolution on core location has been experimentally verified by means of the coincidences with the deep underground muons recorded by MACRO [6]). The resolutions correctly improve with increasing shower size, saturating at  $N_e = 10^6$ , due to the saturation of the photomultipliers recording the particle density nearest to the core. In the same figure the resolution obtained

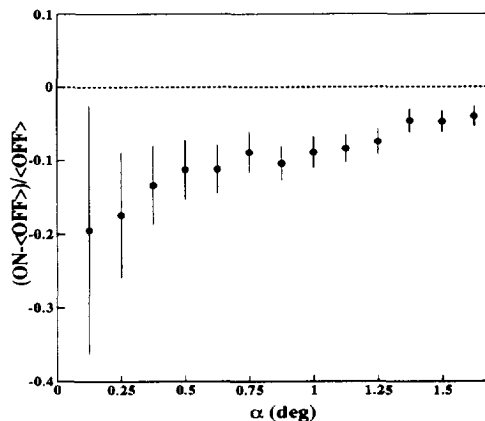


Figure 4. The "moon shadow". The ordinate represents the fractional difference between the number of counts recorded inside a cone of aperture  $\alpha$  around the center of the moon and those measured in two reference regions.

by removing such saturation is also shown, leading to values of:  $\sigma N_e/N_e < 10\%$  and  $\sigma_x = \sigma_y < 2$  m. The fluctuations of the electron number, for primaries of fixed energy and mass number (e.g. protons), is  $\Delta N_e/N_e \approx 20\%$  for  $N_e = 10^6$  (i.e.  $E_0 = 3 \cdot 10^{15}$  eV<sup>1</sup>, corresponding to the "knee" of the primary spectrum); the experimental resolutions are thus smaller than such intrinsic fluctuations.

Resolutions of  $\sigma_\alpha \approx 0.2^\circ$  in the arrival angle, and  $\sigma_x \approx 2$  m in the core location allow the localization of the core of the shower at the depth of the underground laboratories with accuracy of about 4 m, i.e. smaller than the dimensions of the already existing detectors [8,9] and in general of the halls of the underground Gran Sasso laboratories. This partly allows to remove the need of integrating over the core locations in the analysis of coincident events, and moreover provides

<sup>1</sup>The simulated EAS data have been obtained by means of the CORSIKA code [7]. Since the scintillators provide a measurement of "energy losses" rather than of "particle numbers", the response of the e.m. array has been calibrated in primary energy on a 10-50 GeV positron beam at CERN. To have the possibility of comparison with other experiments, the quoted  $N_e$  values have been converted to represent the "total number of charged particles" as usual in EAS experiments.

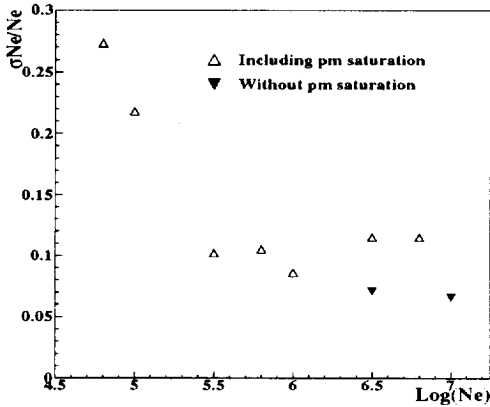


Figure 5. The shower size resolution. The full triangles show the resolution obtained by removing the saturation near the core.

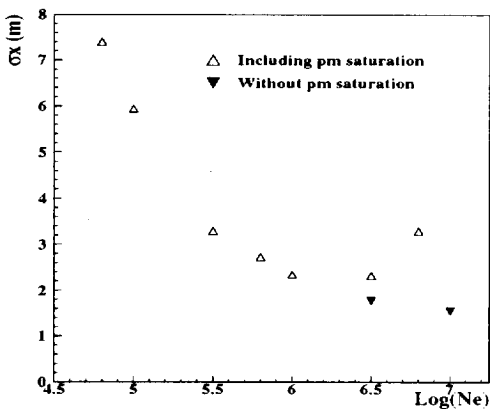


Figure 6. The core location resolution (see also capt. of fig. 5).

a physical significance to individual events with low numbers of detected muons.

## 2.2. The muon detector

The muon detector [10] consists of 9 active planes interleaved by 13 cm thick iron absorbers. The surface of the detector is 140 m<sup>2</sup> and the height 2.8 m. Each plane is made of two layers of streamer tubes for muon tracking and one layer of proportional tubes for hadron calorimetry (see sect. 2.4). Every tube has 3 x 3 cm<sup>2</sup> section and 12 m length. The tracks X coordinates are obtained by the signals of the anode wires,

the Y ones by the induced signals on strips (3 cm width) placed orthogonally to the wires. The muon energy threshold is  $E_\mu \approx 1$  GeV for vertical incidence, the resolution (i.e. the difference between the numbers of visible and reconstructed muons with at least 6 wires and strips fired) is  $\Delta N_\mu^{det}/N_\mu^{det} < 4.3\%$  up to  $N_\mu^{det} = 30$ , and, concerning the angles,  $\Delta\theta_\mu \approx 0.6^\circ$ . Since the core is located by the e.m. array, by using the measured average l.d.f., the total muon number  $N_\mu$  can be obtained; the accuracy is  $\Delta N_\mu/N_\mu \approx 20\%$  at  $N_e \approx 10^6$ .

The effective muon sensitive area is increased by 10 m<sup>2</sup> scintillator detectors positioned below 13 e.m. modules, each shielded by 30 cm of iron.

The primary mass (A) affects the  $N_e$ - $N_\mu$  relation as in the following:

$$N_\mu \approx k \cdot A^{0.2} N_e^{0.8}$$

This holds for all muon energies  $E_\mu$ , provided that  $E_\mu \ll E_0/A$ . Measurements with different muon energies (i.e. muons produced at different stages of the EAS development, or in quite different kinematical regions) provide therefore an important tool to check the hadron cross section used. First data concerning the analysis of the  $N_e$ - $N_\mu^{GeV}$  data in terms of an interaction and a composition model are reported in [11,12]

## 2.3. The coincidences with the deep underground muon detectors

The deep underground detectors LVD [8] and MACRO [9] have surfaces respectively 455 m<sup>2</sup> (182 in operation) and 907 m<sup>2</sup>; the energy threshold for muons reaching their depth (1100 m, 3400 m water equivalent) is  $E_\mu^{th} \approx 1.4$  TeV. Data of the e.m. and Cerenkov EAS-TOP detectors have been reported in coincidences with both underground detectors [6,13–15]. The analysis of the EAS-TOP and MACRO data has shown that the cosmic ray composition is mixed with the presence of both heavy and light components both below and above the “knee” [14] (the quoted  $N_e$ - $N_\mu^{GeV}$  [11,12] and these  $N_e$ - $N_\mu^{TeV}$  data lead independently to similar conclusions).

We want here to discuss the main significance introduced by the threefold coincidence analysis  $N_e$ - $N_\mu^{GeV}$ - $N_\mu^{TeV}$  in the understanding of individ-

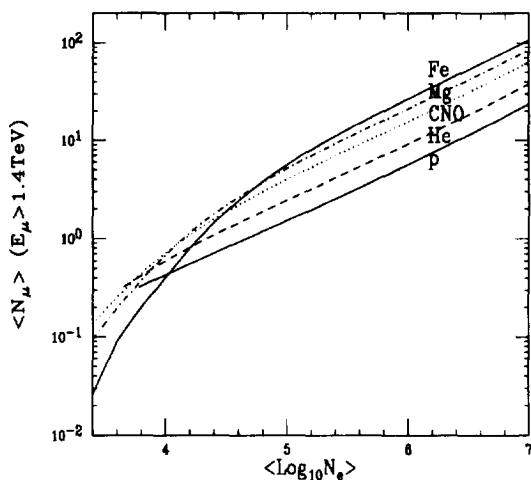


Figure 7. Average TeV muon numbers vs. shower size for different primaries.

ual events. In fact, from the underground data, events due with high probability to heavy (iron type) or light (p, He) primaries can be selected from their high muon multiplicity as compared with their shower size (as e.g. above the iron line in fig. 7) or their high energy in a single muon (see fig. 8). Such events are analyzed at the surface as shown in fig. 9, where the relation  $N_e - N_\mu^{GeV}$  is shown for p and iron primaries of fixed primary energy. The underground selection can be confirmed or rejected, providing thus a constraint to the role of fluctuations and of the uncertainties of the interaction model. As we can see from fig. 9, the fluctuations in  $N_\mu$  for fixed primary energy and e.g.  $A = 56$  are  $\Delta N_\mu / N_\mu \approx 20\%$ , the separation between proton and iron primaries being  $\approx$  factor 2. A resolution better than  $\Delta N_\mu / N_\mu$  is thus required to perform a measurement on individual events. Such statistical accuracy ( $\approx 25$  detected muons) at a typical distance  $\approx 100$  m from the EAS core is now achievable with the EAS-TOP detector at primary energies  $E_0 > E_{knee}$ .

#### 2.4. The calorimetric detector

The GeV muon tracking structure operates as a calorimeter by means of the active layers made

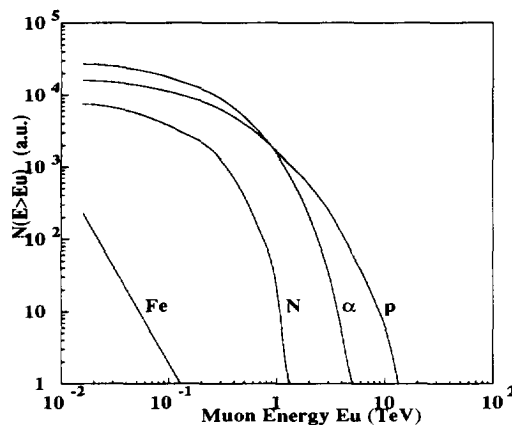


Figure 8. Energy spectrum of muons recorded by a detector located in the deep underground Gran Sasso Laboratories for shower size  $10^5 < N_e < 2 \cdot 10^5$  at the surface.

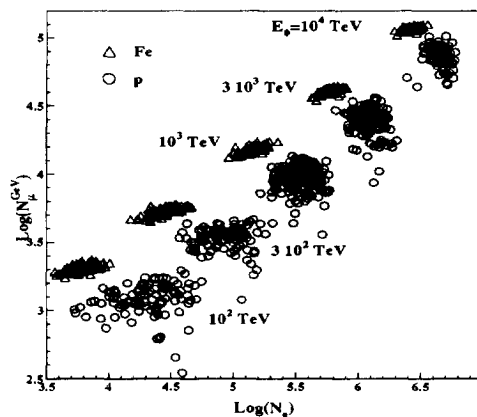


Figure 9.  $N_e - N_\mu$  relation calculated for fixed primary energies and different primaries.

of tubes operating in “quasi proportional” mode (wire thickness  $50 \mu\text{m}$ ,  $V = 2900$  V). The information is read through pads of dimensions  $38 \times 40 \text{ cm}^2$ . The resolution for energy measurement of high energy hadrons is  $\Delta E_h / E_h \approx 30\%$  at  $E_h \approx 1 \text{ TeV}$ . The main informations of interest in this context, for showers with the core hitting the detector, are: a) the measurement of the total energy content in the high energy component in the core (i.e. energy not transferred to the e.m. and muon components as measured at large core distances), and its absorption characteristics; b)

the measurement of the higher energy hadrons; c) the detection of peculiar events as e.g. the multistructured events correlated to large  $P_t$  secondaries produced in hadron interactions [16]. Both informations a) and b) provide selection criteria for given classes of primaries. Rather than on the energy released to the higher energy component as for the criterion discussed in sect. 2.3, the present ones are based on the energy "retained" by the incoming primary, and therefore on different features (total cross sections and inelasticity) of the high energy hadronic process.

## 2.5. The atmospheric Cerenkov light detector

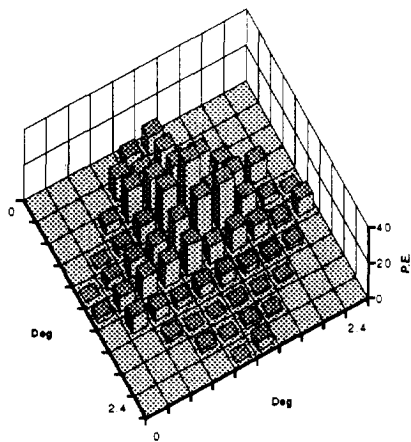


Figure 10a.

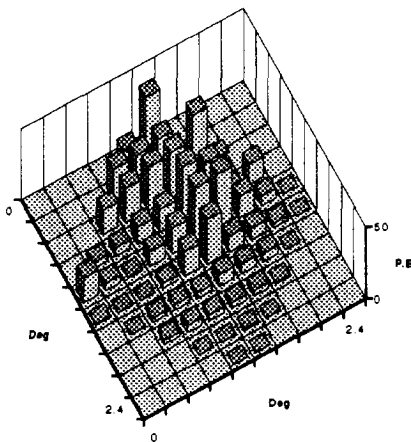


Figure 10b. Cerenkov light images as observed by two multichannel detectors (a,b) close to each other and with parallel fields of view.

The main tool for removing the limitation due to the observation at fixed atmospheric depth is provided by the detection of optical emissions in the atmosphere (fluorescence or Cerenkov light). Fluorescence light can be exploited at primary energies  $E_0 > 10^{17}$  eV. At our energies, Cerenkov light (C.I.) provides the tool for such information, and therefore for the information about the longitudinal development of the shower, that is also related to the rate of energy release in the atmosphere and therefore to the primary composition [17]. A first information can be obtained from the relation  $Q/N_e$  ( $Q$ =total C.I. yield, whose measurement is still dependent on the effective l.d.f. of the C.I. signal). A direct information on the longitudinal EAS development can be obtained from the localization of the altitude of production of the light. This is realized through the determination of the depth of production of the maximum light intensity by means of angular measurements of its direction performed at different core distances<sup>2</sup>.

The Cerenkov light detector of EAS-TOP is made

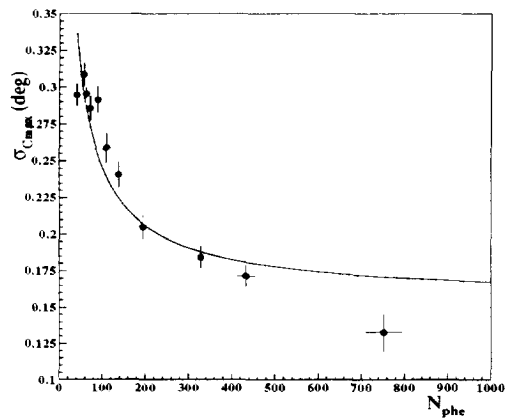


Figure 11. Accuracy in the reconstruction of the direction of the maximum C.I. intensity from a single observation point, as a function of the total number of collected photoelectrons.

<sup>2</sup>The relation between the average depth of shower maximum  $\langle X_m \rangle$ , the primary energy  $E_0$  and the mass number  $A$  is:  $\langle X_m \rangle = C + D \ln(E_0[10^{15} \text{ eV}]/A)$ , where  $C$  and  $D$  depend on the interaction model ( $C \approx 600 \text{ g cm}^{-2}$  and  $D \approx 30 \text{ g cm}^{-2}$ ).

Table 1

Main informations obtained from the multiple measurements performed at EAS-TOP (the energy ranges, besides the physical processes, are determined by the statistics).

| Type of observation               | Energy range (eV)           | Physical information |
|-----------------------------------|-----------------------------|----------------------|
| $N_e - N_\mu^{GeV}$               | $10^{14} - 5 \cdot 10^{16}$ | Composition          |
| $N_e - N_\mu^{TeV}$               | $10^{14} - 10^{16}$         | Composition          |
| $N_e - N_\mu^{GeV} - N_\mu^{TeV}$ | $10^{14} - 5 \cdot 10^{15}$ | Comp.+ Int.          |
| $N_e - N_\mu^{GeV}$ -C.l.img.     | $10^{14} - 10^{15}$         | Comp.+ Int.          |
| $N_e + N_\mu^{TeV}$ +C.l.tot.     | $< 10^{13} - 10^{14}$       | Int. (+ Comp.)       |
| $N_e + N_\mu^{GeV}$ +Calorim.     | $10^{14} - 5 \cdot 10^{15}$ | Spectrum + Comp.     |

of eight telescopes, positioned at  $\approx 100$  m from each other (see fig. 1). Each of them houses three mirrors, 90 cm diameter and 67 cm focal length. One of them is seen by a multichannel photomultiplier (XP 1704, 96 pixels with fields of view  $4.4 \cdot 10^{-5}$  sr each), for image studies. Two of them are seen by arrays of 7 photomultipliers for a full field of view of  $5 \cdot 10^{-2}$  sr, for measurements of the total Cerenkov light signal, and wide acceptance for operating in coincidence with the e.m. and muon detectors. Examples of Cerenkov

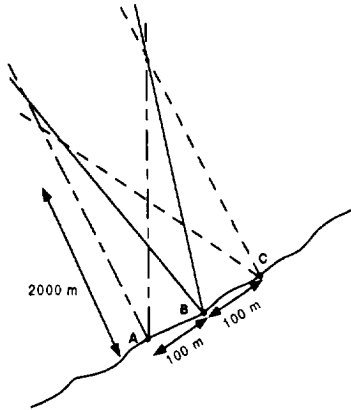


Figure 12. The volume of atmosphere sensitive for the study of the EAS development as seen by the overlapping fields of view of the imaging C.l. detectors (A,B,C; drawing not on scale).

light images as obtained by two imaging detectors mounted on the same support and with parallel

optical axis are shown in fig 10 (a,b). The accuracy in the reconstruction of the direction from which the maximum of light is detected, is shown in fig. 11 as a function of the total number of collected photoelectrons [21]. It depends on the total number of detected photons as expected from the poissonian fluctuations, and it saturates at  $< 0.2^\circ$ . Such accuracy implies for the determination of the height of EAS maximum, with 8 observation points, a resolution of about  $40 \text{ g cm}^{-2}$  (the average difference in the depth of EAS maximum for proton and iron primaries is  $\approx 100 \text{ g cm}^{-2}$ ). With the present fields of view, in two years of data taking, the energy range up to  $10^{15}$  eV can be studied. A detection scheme is shown in fig. 12: the effective sensitive volume of atmosphere has surface  $S \approx 10^4 \text{ m}^2$ , from  $h_{min} \approx 2000$  m above the detector to  $h_{max} \approx 7000 - 8000$  m where the resolution is reduced of a factor  $\approx 2$  (the relevant heights of interest are between 3000 and 6000 m above the detector).

As shown by the event reported in fig 10, the agreement between the full images recorded by the two detectors is fairly good, thus showing that additional informations can be extracted from the number of photoelectrons recorded by individual pixels [21]. In fact the fluctuations in the measurement of the photoelectron content of each  $0.2^\circ \times 0.2^\circ$  pixel is  $\approx 20\%$  beside poissonian fluctuations.

From another point of view, the majority of muons recorded by the deep underground detectors are produced by primary protons of energy  $E_0 \approx 5 \text{ TeV}$ . At such energies only primary protons, whose flux is known from the direct measurements, can contribute to the TeV under-

ground muon flux. The atmospheric Cerenkov light yield associated to the TeV muons provides therefore a new tool for calibrating the simulations and checking the cross section for pion production in the forward region at  $E_\mu \approx E_0/A$ . The performed tests [13,15] have shown that the measurement is possible.  $E_0$  is measured with accuracy  $\approx 20\%$ , and at higher energies the data are sensitive to the ratio "alfa/p" in the primary beam [22].

### 3. CONCLUSIONS

By means of the multiparametric EAS-TOP array operating at the Gran Sasso laboratories, also in connection with the deep underground muon detectors, well defined samples of high energy cosmic ray events are obtained in different energy ranges. This allows to face specific items in the spectra-composition- interaction models puzzle concerning the cosmic ray radiation around the "knee" of the primary energy spectrum. The fields of main significance of the different measurements are summarized in tab. 1.

### REFERENCES

1. M. Aglietta et al, Il Nuovo Cimento, 9C (1986) 262
2. M. Aglietta et al, Nuclear Instr. Meth. in Phys. Res., A277 (1989) 23
3. M. Aglietta et al, Nuclear Instr. Meth. in Phys. Res., A336 (1993) 310
4. M. Aglietta et al, AIP Conference Proc. 220, High Energy Gamma-Ray Astronomy (Ann Arbor, 1990) 145
5. M. Aglietta et al, Proc. 22nd I.C.R.C., 2 (Dublin, 1991) 708
6. R. Bellotti et al, Phys. Rev. D, 42 (1990) 1396
7. J.N. Capdevielle et al, KfK Report 4998 (Karlsruhe, 1992)
8. M. Aglietta et al (LVD Coll.), Astroparticle Physics, 2, 103 (1994)
9. S.P. Ahlen et al, Nucl. Instr. and Meth. in Phys. Res. A, 324, 337 (1993)
10. EAS-TOP Coll., Proc. 23rd I.C.R.C., 4 (Calgary, 1993) 251
11. EAS-TOP Coll., Proc. 24rd I.C.R.C., 2 (Roma, 1995) 664
12. M. Aglietta et al, Il Nuovo Cimento (1996) in press
13. EAS-TOP and MACRO Coll., Proc. 2nd Int. Workshop on Neutrino Telescopes, 209 (Venezia, 1990)
14. M. Aglietta et al, Physics Letters B, 35 (1994) 376
15. M. Aglietta et al, Il Nuovo Cimento C, 15 (1992) 357
16. M. Aglietta et al, Il Nuovo Cimento C, 18 (1995) 663
17. J. Linsley, Ap. J., 235 (1980) L167
18. M. Aglietta et al, Il Nuovo Cimento C, 16 (1993) 813
19. M. Aglietta et al, Proc. 24rd I.C.R.C., 1 (Roma, 1995) 430
20. M. Aglietta et al, Proc. 24rd I.C.R.C., 1 (Roma, 1995) 434
21. M. Aglietta et al, Astroparticle Physics (1996) in press
22. M. Aglietta et al, Il Nuovo Cimento, "Topics in Cosmogeophysics", 247 (1995)